RSC Advances

PAPER

View Article Online
View Journal | View Issue

CrossMark click for updates

Cite this: *RSC Adv.*, 2016, **6**, 94193

From diffusive to ballistic Stefan–Boltzmann heat transport in thin non-crystalline films†

A. Makris, T. Haeger, R. Heiderhoff* and T. Riedl

Today, different theoretical models exist to describe heat transport in ultra-thin films with a thickness approaching the phonon mean free path length. Due to the influence of parasitic effects, the experimental assessment of heat transport in these ultra-thin films with the required sensitivity is extremely challenging. In this work, the heat transport through thin non-crystalline metal-oxide films is studied using scanning near-field thermal microscopy, which allows to minimize parasitic thermal effects and therefore provides uttermost sensitivity even for the study of thermal transport in ultra-thin films. For the first time, we provide experimental evidence of enhanced out-of-plane heat dissipation in these ultra-thin metal-oxide films by ballistic thermal phonon transport according to the Stefan–Boltzmann-like heat transport model.

Received 12th August 2016
Accepted 23rd September 2016

DOI: 10.1039/c6ra20407d

www.rsc.org/advances

Open Access Article. Published on 03 October 2016. Downloaded on 6/5/2026 9:49:26 AM.
This article is licensed under a Creative Commons Attribution 3.0 Unported Licence.

Introduction

In electrical insulators, phonons are the predominant species for heat transport. For bulk materials the heat flux $\vec{q}$ is classically described by the Fourier law,[1] where in general $T(\vec{r})$ is a given temperature distribution and $\overleftrightarrow{\lambda}$ is the tensor of thermal conductivity:[2]

$$\vec{q} = -\overleftrightarrow{\lambda}\ \mathrm{grad}\ T(\vec{r}) \tag{1}$$

There are steady state as well as transient techniques within the space and time/frequency domain to analyze thermal transport.[3–7] If the absorbed power in the sample is known, the thermal conductivity can be directly determined in steady state approaches. In the dynamic case, the density ρ as well as the specific heat c of the material must be considered. Heat flow is described by the general equation of heat conduction:[8]

$$\rho c \frac{\partial T(\vec{r})}{\partial t} = \frac{\partial}{\partial x}\left(\lambda_x \frac{\partial T(\vec{r})}{\partial x}\right) + \frac{\partial}{\partial y}\left(\lambda_y \frac{\partial T(\vec{r})}{\partial y}\right) + \frac{\partial}{\partial z}\left(\lambda_z \frac{\partial T(\vec{r})}{\partial z}\right) + q_E \tag{2}$$

here, q_E indicates the heat generation per unit time and unit volume. The heat can be generated for example by a laser, by heated resistive metal strips directly deposited onto the sample, *etc.* Since only the time derivative of $T(\vec{r})$ appears in this equation, the knowledge of the absolute temperature and the absorbed power is not required. To get access to the three-dimensional material property $\overleftrightarrow{\lambda}$, directional heat transport investigations have been carried out using various experimental techniques.[7]

Furthermore, the heat flux strongly depends on the dimensions of the materials and is of growing general interest in the case of a shrinking device size and in thin film technology. Hence, films on substrates with either low or high thermal conductivity have been investigated in order to study in-plane or out-of-plane (also called cross-plane) heat flux (Fig. 1).[7]

While there is extensive experimental work on the in-plane heat transport in thin films down to film thicknesses of around 20 nm, it must be pointed out that out-of-plane transport is experimentally far less explored and studies are typically limited to film thicknesses larger than 100 nm.[9–14] Within these works, a decrease of the thermal conductivity with decreasing film thickness d_{film} from 2 μm (ref. 15) to 300 nm (ref. 16) has been found for dielectrics and semiconductors. On the contrary, we have found the thermal conductivity of an organic Alq_3 thin film with d_{film} down to 20 nm to be constant.[17]

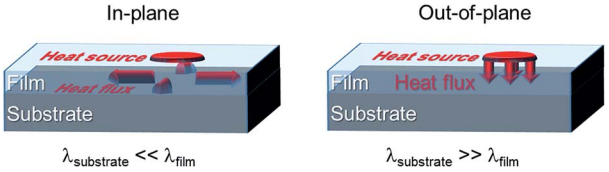

Fig. 1 Schematic illustration of in-plane and out-of-plane heat transport.

Institute of Electronic Devices, University of Wuppertal, Rainer-Gruenter-Str. 21, 42119 Wuppertal, Germany. E-mail: heiderho@uni-wuppertal.de

† Electronic supplementary information (ESI) available: Details of thin film preparation, scanning near-field thermal microscopy, Stefan–Boltzmann like heat transfer. See DOI: 10.1039/c6ra20407d

Open Access Article. Published on 03 October 2016. Downloaded on 6/5/2026 9:49:26 AM.
This article is licensed under a Creative Commons Attribution 3.0 Unported Licence.

For ultra-thin films with a film thickness below the phonon mean-free path Λ (*i.e.* $d_{\text{film}} < \Lambda$), also referred to as Casimir limit,[18] some further ambiguities exist. In some reports, these ultra-thin films are considered to be thermal insulators, where phonons are claimed to be trapped between the layer boundaries. Trapped phonons are not able to transport thermal energy.[10] In addition the Fourier law is no longer valid in the case of heat source dimensions to values smaller than Λ, which can be hundreds of nanometers in crystalline materials at room temperature.[19] A significant decrease in energy transport occurs even into bulk material at nanoscale heated regions compared with Fourier-law predictions due to quasi-ballistic thermal transport effects (quasi-ballistic: with and without scattered phonons). On the contrary could be demonstrated, that surface phonon polaritons excited by a laser beam dramatically enhance energy transfer between two surfaces at small gaps (30 nm) by measuring radiation heat transfer between a microsphere and a flat surface.[20] An extremely enhanced heat flux by blackbody radiative transfer of energy from the heater can only be considered under extreme near-field conditions. Although experimental advances have enabled elucidation of heat transfer in gaps as small as 20 nm, quantitative analysis of enhanced radiative heat transfer in the extreme near-field (gaps less than 10 nm) have been carried out just very recently.[21] By a similar token, theoretical work based on the Boltzmann transport equation (BTE) for films with $d_{\text{film}} < \Lambda$ (below the Casimir limit) considered heat transport to be ballistic and resulted in a description similar to that known from radiative heat transport according to the Stefan–Boltzmann law.[22–24] As of yet, the experimental verification of this theory is missing.

In this paper, we study out-of-plane heat transport from a nanoscale heat source through ultra-thin non-crystalline metal-oxide films, *e.g.* Al_2O_3 and TiO_2, with a thickness down to 4 nm by means of dynamic scanning near-field thermal microscopy (SThM). We have prepared our ultra-thin amorphous like films by atomic layer deposition (ALD), as it is known to allow for uttermost control of layer thickness, conformity, and homogeneity confirmed by former X-ray diffraction and transmission electron microscopy studies.[25] For the first time, we provide experimental evidence that the out-of-plane heat transport in ultra-thin films is dominated by ballistic heat transport and can therefore be described by a Stefan–Boltzmann like model.

Experimental

For the out-of-plane heat transport analysis we used silicon as substrate material with a relatively high thermal conductivity of 150 W (m^{-1} K^{-1}). Non-crystalline Al_2O_3 and TiO_2 films were prepared in a step-like matrix (Fig. 2), where all films exhibited a direct step from the film to the Si-substrate to directly assess the heat flux through the film for each film thickness as described below.

The SThM in the present work is installed in the analysis chamber of an Environmental Scanning Electron Microscope (ESEM), thus our SThM measurements are carried out under vacuum (5×10^{-6} mbar).[26] Effects of thermal transport due to convection or moisture related interfacial effects can therefore be excluded. The signal detection in our specific setup has been explained in detail elsewhere.[27] Briefly, we applied a transient measurement technique within the frequency domain thus only the derivative of $T(\vec{r}, \omega)$ in the swung-in state will be discussed in the following. A constant low force between SThM probe and sample was applied during these measurements to guarantee a constant resulting thermal contact resistance and in order to prevent mechanical influences/damages to the films. Further details can be found in the ESI.†

The resistive thermal probe of the SThM is powered by an AC current $I_0 \sin(\omega t)$ with angular frequency ω. As demonstrated earlier,[28,29] the probe can be considered in far-field as a point like heat source and in close proximity as a line-shaped nanoscale heat source fulfilling the demands for high resolution near-field microscopy[30] by generating a heat wave of frequency 2ω with cylindrical symmetry. This wave will diffuse into the substrate and is exponentially damped in the radial direction. According to Carslaw and Jaeger, the resulting amplitude of the temperature oscillations $\hat{T}(r)$ in the sample at a distance r from the heat source depends on the amplitude of the generated heat power $\hat{P}$ per unit length flowing into the sample and the thermal conductivity λ as:[31]

$$\hat{T}(r,\ \omega) = \frac{\hat{P}}{\pi\lambda} K_0(\sigma(\omega),\ r) \tag{3}$$

K_0 is the zeroth-order modified Bessel function and $\sigma(\omega)$ defines the complex thermal wave number accounting for a phase difference between temperature and AC heating power of the source. The magnitude of the complex quantity $1/\sigma(\omega)$ is the thermal penetration depth, *i.e.* the characteristic depth of heat diffusion during one cycle of the ac power heating the sample. According to Cahill[31] and Fiege *et al.*[32] in SThM, one may approximate:

$$\hat{T}(r,\ \omega) = \frac{\hat{P}}{\pi\lambda}\left(\ln(2) - 0.5772 - \frac{\mathrm{j}\pi}{4} + \frac{1}{2}\ln\left(\frac{a}{r^2}\right) - \frac{1}{2}\ln(\omega)\right) \tag{4}$$

here, $a = \lambda/\rho c$ denotes the thermal diffusivity of the material. Since heater and thermometer are combined in one element, the thermal conductivity of the sample can be determined quantitatively by keeping $\hat{P}$ constant and measuring the resulting 3ω component of the voltage drop across the SThM probe $\hat{U}_{3\omega}$ at two different frequencies ω_1 and ω_2.

$$\frac{\hat{U}_{3\omega_1} - \hat{U}_{3\omega_2}}{\ln(\omega_1) - \ln(\omega_2)} = \frac{\hat{P}}{\pi\lambda}\frac{1}{4} I_0 \frac{\mathrm{d}R}{\mathrm{d}T} \tag{5}$$

The term $\frac{\mathrm{d}R}{\mathrm{d}T}$ represents the differential thermal coefficient of the probe.

Unfortunately, in SThM $\hat{P}$ depends on the thermal properties (*e.g.* thermal conductivity)[27,33] of both the sample and the probe design. This means that factors like heat dissipation into the supply lines of the thermal probe *etc.* must also be considered. Furthermore, the heat transfer mechanisms between the probe and the sample must be calibrated. The tip-sample thermal

 This journal is © The Royal Society of Chemistry 2016

Open Access Article. Published on 03 October 2016. Downloaded on 6/5/2026 9:49:26 AM.
This article is licensed under a Creative Commons Attribution 3.0 Unported Licence.

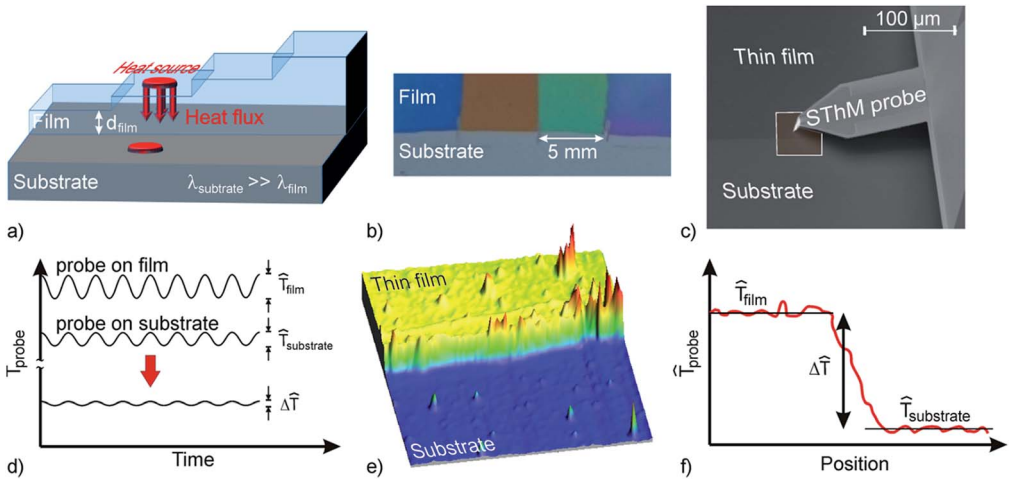

Fig. 2 Thermal analysis on an ALD deposited step-like film matrix. (a) The step-like matrix allows to measure a direct difference of heat flux between different film thicknesses to the substrate. (b) Optical top-view image of the matrix showing different layer thicknesses in different colors due to interference effects. (c) SEM image of the SThM probe positioned at the edge of a substrate and film (d) schematic diagram of changes of the probe temperature in the SThM measurement (for details, please see discussion in text). The peak to valley distance of the temperature oscillation for the tip on top of the film, substrate is denoted by the so-called temperature oscillations $\hat{T}_{film}$, $\hat{T}_{substrate}$, $\Delta\hat{T}$ denotes the difference $\hat{T}_{film} - \hat{T}_{substrate}$ (c) resulting temperature oscillation detected at a frequency of 3.3 kHz (40 µm × 40 µm). (f) Schematic that shows the temperature oscillation $\hat{T}_{probe}$ *vs.* position. The absolute difference $\Delta\hat{T}$ is obtained by averaging the scan signals (shown in e).

contact resistance can be affected by heat conduction and thermal radiation near the contact region as discussed in detail by Wilson *et al.*[33] in order to perform thermal conductivity measurements in the 3ω mode using a Wollaston wire. This renders the application of the conventional 3ω method difficult for the quantitative determination of thermal conductivity in dependence on the film thickness using VITA-SThM probes. Thus, in order to perform measurements of out-of-plane heat transport from a nanoscale heat source through thin films, we determine the difference of the amplitude of the temperature oscillations of the probe on the film and on the substrate $\Delta\hat{T} = \hat{T}_{film} - \hat{T}_{substrate}$ as illustrated in Fig. 2.

Out-of-plane heat dissipation in thin non-crystalline metal-oxide films

Diffusive out-of-plane heat transport. As the silicon substrate has a relatively high thermal conductivity, $\hat{T}_{substrate}$ is relatively small (eqn (3)). If the amplitude of electrical power supplied to the probe is kept constant and if only diffusive heat transport in a film with low thermal conductivity is assumed, the temperature oscillation of the probe on top of the film $\hat{T}_{film}$ is larger than $\hat{T}_{substrate}$. In the limit where the thermal conductivity of a film would trend to zero, no heat would diffuse into the film. In this case, the generated joule heat would exclusively be transported away from the SThM probe *via* its supply lines.

An exemplary result of $\Delta\hat{T}$ *vs.* d_{film} for Al_2O_3 films is shown in Fig. 3. The uncertainties of temperature and film thickness measurements (for films below 30 nm) are ±0.5 K and $\pm d_{film}$ 10% nm respectively.

To understand the dependence of $\Delta\hat{T}$ *vs.* d_{film}, different regimes of thermal transport must be considered. For d_{film} > 100 nm, $\Delta\hat{T}$ saturates at a level $\Delta\hat{T}_{max}$, which indicates that in this regime the Al_2O_3 layer can be considered as bulk material. Thus, heat transport is diffusive and follows the Fourier law.[2] Using the 3ω-technique here (see eqn (5)), we determined the thermal conductivity to $\lambda_{Al_2O_3} = 0.8$ W m^{-1} K^{-1} on an average film thickness of 338 nm ± 5 nm using the line source model of the probe. This value is in agreement with previous reports for ALD grown non-crystalline Al_2O_3 layers.[34] The advantages of this 3ω-technique on thermal conductivity analyses of amorphous solids are discussed in detail elsewhere.[35] Towards thinner films (d_{film} < 100 nm), $\Delta\hat{T}$ decays and finally levels off for d_{film} < 30 nm.

Lee and Cahill[16] used a one-dimensional description to model the out-of-plane heat flow through a film with thicknesses d_{film} far less than the thermal penetration depth and much smaller than the width of the heater/thermometer w. If

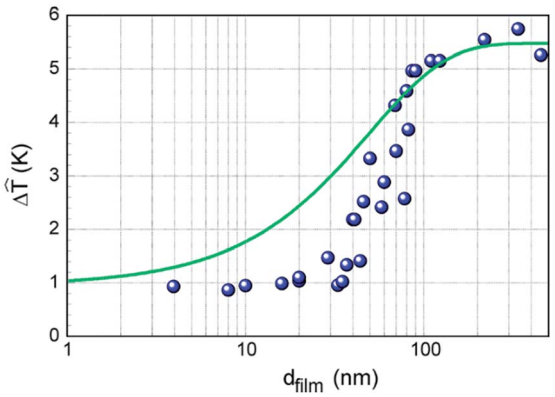

Fig. 3 Comparison of measured and calculated $\Delta\hat{T}$ of Al_2O_3 films in dependence on the film thickness. The calculated curve is a result of eqn (8) with $\hat{T}_{contact} = 1$ K.

Open Access Article. Published on 03 October 2016. Downloaded on 6/5/2026 9:49:26 AM.
This article is licensed under a Creative Commons Attribution 3.0 Unported Licence.

the thermal conductivity of the film is substantially smaller than that of the substrate, this model yields a linear relation of $\Delta\hat{T}$ and d_{film} as follows:

$$\Delta\hat{T}(d_{\mathrm{film}}) = \frac{\hat{P}}{w\lambda_{\mathrm{film}}} d_{\mathrm{film}} \tag{6}$$

A frequency independent offset of a temperature oscillation amplitude $\Delta\hat{T}$ is added to the thermal 3ω response of the substrate. Note, as $\Delta\hat{T}$ scales with d_{film}/w, the measurement of ultra-thin films with microscopic probes ($d_{\mathrm{film}} \ll w$) becomes very challenging. This might be the reason why the out-of-plane heat transport is less explored for ultra-thin films using macroscopic probes (with a large w).[9,10] On the other hand, in the case of a SThM the ultra-small w on the order of 50 nm (ref. 36) should be perfectly suited to assess thermal transport in ultra-thin films.

It is not directly obvious from eqn (6) that $\hat{T}_{\mathrm{film}}$ would become independent of d_{film} for ultra-thin films (d_{film} < 30 nm in the example shown in Fig. 3). According to eqn (6), the region of constant $\Delta\hat{T}$ could be indicative of a thickness dependent thermal conductivity: $\lambda_{\mathrm{film}} \propto d_{\mathrm{film}}$. This assumption would lead to the conclusion, that ultra-thin films become thermal insulators, as claimed by Lee and Cahill.[16] Later Lee and Cahill revised this model by introducing a thermal contact resistance ($R_{\mathrm{resistive}}$) to be responsible for the observation of $\hat{T}_{\mathrm{film}}$ becoming constant.[16] They assumed an apparent thermal conductivity λ_{a} which depends on the film thickness d_{film}, the thermal resistance $R_{\mathrm{resistive}}$ and the intrinsic thermal conductivity λ_{i}:

$$\lambda_{\mathrm{a}} = \frac{\lambda_{\mathrm{i}}}{1 + \frac{R_{\mathrm{resistive}}\lambda_{\mathrm{i}}}{d_{\mathrm{film}}}} \tag{7}$$

As we will discuss below this assumption does not allow us to explain our experimental results shown in Fig. 3.

The transition from thin films to bulk materials (including transition from one-dimensional heat transport across the film to three-dimensional heat transport in bulk material) has been described by the introduction of a saturating exponential function,[17] that for a given frequency ω finally leads to:

$$\Delta\hat{T}(d_{\mathrm{film}}) = \Delta\hat{T}_{\max}\left(1 - \mathrm{e}^{-\frac{d_{\mathrm{film}}}{2r_{\mathrm{contact}}}}\right) + \hat{T}_{\mathrm{contact}} \tag{8}$$

here, $\Delta\hat{T}_{\max}$ is the difference of temperature oscillation ($\hat{T}_{\mathrm{film}} - \hat{T}_{\mathrm{substrate}})_{\max}$ found in the limit of thick films, r_{contact} is the radius of the effective contact area of the probe, and $\hat{T}_{\mathrm{contact}}$ is the temperature offset caused by a constant thermal contact resistance, as r_{contact} and the thermal contact resistance are constant for a certain range of sample thermal conductivity[33] which is typically neglected in eqn (6). Note, aside from $\hat{T}_{\mathrm{contact}}$, in the limit of ultra-thin films (one-dimensional heat transport) eqn (8) becomes identical to eqn (6) (assuming $w = 2r_{\mathrm{contact}}$ and $\Delta\hat{T}_{\max} = \frac{\hat{P}}{\lambda_{\mathrm{film}}}$ as frequency independent). As the radius of an effective contact area of the probe is known to be on the order of 50 nm and $\Delta\hat{T}_{\max}$ was measured to be approximately 5.5 K in the measurement shown in Fig. 3, $\Delta\hat{T}(d_{\mathrm{film}})$ can be derived from eqn (8). Note, $\frac{\hat{P}}{\lambda_{\mathrm{film}}}$ is assumed to be constant and we set $\hat{T}_{\mathrm{contact}} = 1$ K. Obviously, this calculation only fits to the measurement for film thicknesses larger than 80 nm (a similar treatment for TiO_2 thin films can be found in the ESI†). The deviation of calculation and measurement indicates a substantially higher heat flux for thinner films (d_{film} < 80 nm) than expected by eqn (8). We want to stress that the previous assumption of a thickness dependent thermal conductivity ($\lambda_{\mathrm{film}} \propto d_{\mathrm{film}}$) as well as a decrease of the effective λ_{film} calculated recently by a variational approach to solving the BTE[24] does not allow for a better fit to the data, but this assumption would rather increase the deviation.

Note, phonon trapping between the layer boundaries affecting the thermal conductivity at a film thickness on the order of $d_{\mathrm{film}} = 30$ nm as well as a decrease of the effective λ_{film} is not very likely in our samples, as the phonon mean free path is estimated to be approximately two orders of magnitude less for non-crystalline Al_2O_3 ($\Lambda_{Al_2O_3} = 0.47$ nm) and $\Lambda_{Al_2O_3} = 3.5$ nm for sintered polycrystalline Al_2O_3.[37]

Out-of-plane Stefan–Boltzmann-like heat dissipation by ballistic thermal phonon transport. An alternative explanation for the constant $\Delta\hat{T}$ towards ultra-thin films and for the elevated higher heat flow in the region below 80 nm could be related to a constant thermal contact resistance and a significant contribution of Stefan–Boltzmann like heat transport of phonons (which cannot be described by the classical eqn (3)–(8) for diffusive heat transport). It has to be noted, that our measurements are carried out under vacuum conditions, thus heat transport by convection and other parasitic mechanisms related to air and moisture are negligible. Furthermore, effects of radiative blackbody heat transfer are only important in the extreme near-field at a distance far less than 10 nm (ref. 21) and for elevated probe temperatures significantly above those used in our experiment (<400 K).

In order to prove Stefan–Boltzmann like heat transfer of phonons the SThM probe temperatures were measured at different applied electrical powers P_{electr} to heat the probe. The temperatures were detected under steady state conditions for the SThM probe in vacuum (T_{vac}) and in contact on a 10 nm thick film (T_{film}), respectively (Fig. 4a). This thickness was used to avoid a thermal flux due to blackbody radiative heat transport (for gaps less than 10 nm), and to guarantee one dimensional heat transport across the film, as well as to keep contributions due to diffusive heat transport (in case of TiO_2 for d_{film} > 17 nm) negligible.

Thereby, the heat dissipated into the supply lines of the thermal probe can be taken into consideration as the same electrical power P_{electr} is supplied to the SThM probe in vacuum and when in contact with the film (more details are available in the ESI†). At moderate temperatures the thermal capacity of the supply line of the thermal probe C_{suppl} is temperature independent and the radiation heat transfer between our probe and chamber walls is negligible (see ESI†). Finally we derive:

 This journal is © The Royal Society of Chemistry 2016

Open Access Article. Published on 03 October 2016. Downloaded on 6/5/2026 9:49:26 AM.
This article is licensed under a Creative Commons Attribution 3.0 Unported Licence.

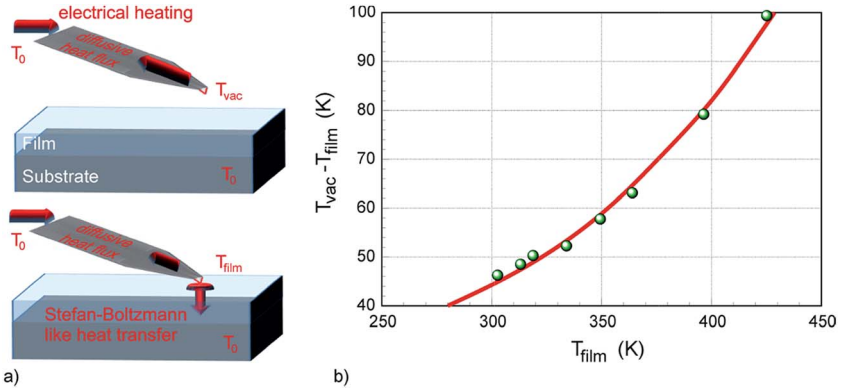

Fig. 4 Experimental setup to verify ballistic heat transport in case of a 10 nm thick Al_2O_3 film. (a) Measured ($T_{vac} - T_{film}$) plotted *vs.* T_{film} (b). The solid line represents a fit assuming Stefan–Boltzmann-like heat transport, *i.e.* $(T_{vac} - T_{film}) = (26.9 \pm 1.3)\ K + (2.1 \pm 0.1)10^{-9}\ K^{-3}\ T_{film}^4$.

$$\lambda_{suppl}\frac{A_{suppl}}{l_{suppl}}\left(T_{vac}-T_{film}\right)=e^{-\frac{d_{film}}{\Lambda_{film}}}\sigma A_{contact}^{Stefan-Boltzmann}\left(T_{film}^{4}-T_{0}^{4}\right) \quad (9)$$

here, λ_{suppl}, A_{suppl}, and l_{suppl} are the effective thermal conductivity, the cross-sectional area, and the length of the supply lines and T_0 is the ambient temperature in the lab (room temperature, thermal reservoir). The term on the right describes the Stefan–Boltzmann like contribution of phonons multiplied with its relative weight given by the ratio of film thickness and phonon mean free path (*i.e.* $e^{-\frac{d_{film}}{\Lambda_{film}}}$).[22] $A_{contact}^{Stefan-Boltzmann}$ is the effective contact area for ballistic heat transport. σ is the Stefan–Boltzmann constant for phonons, which can be related to the specific heat,[31] the temperature, and the velocities of sound,[38] which depends on the pressure.[39] Thus, as described before in the "Experimental" section, the leading force of the probe was kept as low as possible and moderate SThM temperatures were used.

Stefan–Boltzmann like heat transport of phonons is becoming more dominant with decreasing film thickness according to the calculations presented in the ESI.† To prove the validity of this Stefan–Boltzmann model for the heat transport in our ultra-thin films we measured T_{film} at varied electrical heating powers P_{electr}, applied to the thermal probe (see Fig. 4b). As can be concluded from the graph, which was reproducibly obtained on different scan-areas for an Al_2O_3 film with $d_{film} =$ 10 nm, there is an excellent fit of $(T_{vac} - T_{film}) \sim T_{film}^4$. A temperature offset of the SThM probe in vacuum is related to the laser heating of the deflection method for obtaining the topography. In this case the scattering of the measured data is attributed to different scan-areas of our SThM probe on the film. This agreement, for the first time provides clear experimental evidence that the out-of-plane heat transport mechanism from a nanoscale heat source in ultra-thin films is dominated by ballistic heat transport of phonons and can be described by a Stefan–Boltzmann like model. In the discussion of $\Delta\hat{T}$ *vs.* d_{film} (Fig. 3), the regime of ultra-thin films is therefore dominated by Stefan–Boltzmann like heat transport. It should be noted that the contribution of ballistic heat transport is dominant even when the probability of Stefan–Boltzmann like transport is relatively small. The $\hat{T}_{contact}$ found in this case is associated with ballistic heat transport through $A_{contact}^{Stefan-Boltzmann}$. With increasing film thickness, the contribution of ballistic transport decreases exponentially. This will finally lead to a significant increase of $\Delta\hat{T} > \hat{T}_{contact}$ with increasing film thickness (>30 nm) as observed in our previous measurements (Fig. 3).

From diffusive to ballistic Stefan–Boltzmann-like out-of-plane heat transport. As the relative contribution of Stefan–Boltzmann heat transport depends exponentially on d_{film}, the phonon mean free path Λ_{film} can be estimated from the transition of the dominating ballistic regime, which is indicated by a constant $\Delta\hat{T} = \hat{T}_{contact}$, to the regime where heat transport through the thin film will become increasingly diffusive (Fig. S3†). The film thickness for which the contribution of diffusive and ballistic thermal transport is equal can be determined to be $d_{film} = 26$ nm in the case of Al_2O_3 and $d_{film} = 17$ nm for TiO_2.

In this context, the contribution of various phonon modes must be taken in to account in the Stefan–Boltzmann like heat transfer, as already discussed especially for amorphous materials.[40] Note, in our case is $d_{film} \gg \Lambda_{film}$. Consequently we considered the non-crystalline films with $d_{film} > 4$ nm as bulk materials. Hence, in comparison to acoustic phonons the contribution of optical phonons to the thermal transport is negligible at room temperature.[41] Finally, it should be noted that optical phonons, which are usually neglected in thermal conduction for their relatively small group velocities compared with acoustic phonons, can significantly enhance heat transport at room temperature in extremely thin films ($d_{film} < \Lambda_{film}$).[42]

At low temperatures and in isotropic condensed matter, σ was already calculated by Swartz and Pohl[38] in studies of thermal boundary resistances and is given by:

$$\sigma = \frac{\pi^2 k_B^4}{120\hbar^3}\sum_i \frac{1}{c_i^2} \quad (10)$$

here, k_B is Boltzmann's constant, $\hbar$ is the reduced Planck constant, and c_i is the velocity of sound in longitudinal and transverse direction. While transverse acoustic phonons are the primary carriers of energy at low temperatures (T < 200 K),

Open Access Article. Published on 03 October 2016. Downloaded on 6/5/2026 9:49:26 AM.
This article is licensed under a Creative Commons Attribution 3.0 Unported Licence.

longitudinal acoustic phonons carry more energy at higher temperatures.[43] Finally, Λ_{film} of longitudinal acoustic phonons can be estimated from the transition where diffusive and ballistic thermal transport is equal by use of eqn (9) and (10) to:

$$\Lambda_{film} = -\frac{d_{film}}{\ln\left[\left(\frac{120\hbar^3 {c_{longitudinal}}^2 \lambda_{film}}{\pi^2 {k_B}^4 d_{film}}\right)\frac{(T_{film}-T_0)}{\left({T_{film}}^4-{T_0}^4\right)}\right]} \quad (11)$$

Λ_{film} has been determined to be 0.63 nm and 0.43 nm at longitudinal sound velocities $c_{longitudinal}$ of 8700 m s^{-1} (ref. 44) and 10 375 m s^{-1} (ref. 45) for Al_2O_3 and TiO_2 respectively, in the limit $T_{film} \rightarrow T_0$. The values for Λ_{film} of Al_2O_3 and TiO_2 are comparable to that found in literature of 0.47–3.5 nm for Al_2O_3 (ref. 37) and of 0.4–1 nm for TiO_2.[46]

Conclusions

In summary, we performed out-of-plane heat transport measurements of a nanoscale heat source through thin non-crystalline Al_2O_3 and TiO_2 films for thicknesses from 450 nm down to 4 nm by use of scanning nearfield thermal microscopy (SThM). No change of the thermal conductivity and a pure diffusive heat transport were found for Al_2O_3 films with a thickness larger than 80 nm. At decreasing film thicknesses a significant enhancement of heat transport was detected, which could not be explained by diffusive thermal transport alone. As we have clearly evidenced for the first time, in this regime heat dissipation has a significant contribution of ballistic Stefan–Boltzmann like heat transport of phonons. From the transition of dominating ballistic out-of-plane heat transport to increasing probability of diffusive mechanism the mean-free path of longitudinal acoustic phonons have been estimated to be 0.63 nm and 0.43 nm for Al_2O_3 and TiO_2 respectively.

These results will significantly influence thin film technology and the thermal management of modern devices, as heat dissipation is at this time the key limiting factor for power electronics, including high-power RF devices as well as in high-power laser diodes and high-brightness light-emitting diodes (LEDs). In contradiction to former estimations, that ultra-thin films become thermal insulators, an enhanced heat dissipation by ballistic phonon transport occurs with decreasing film thicknesses even far above the Casimir limit.

Acknowledgements

This work was supported by the Deutsche Forschungsgemeinschaft (DFG) under the project number HE2698/7-1.

References

1 J. B. J. Fourier, *Theorié analytique de la chaleur*, Chez Firmin Didot, père et fils, 1822.
2 A. Freeman, *Theory of heat*, Cambridge University Press, London, 1878.
3 R. Heiderhoff, A. Makris and T. Riedl, *Mater. Sci. Semicond. Process.*, 2016, **43**, 163–176.
4 Z. L. Wu, M. Reichling, X. Hu and K. Balasubramanian, *Appl. Opt.*, 1993, **32**, 5660–5665.
5 D. M. Price, M. Reading, A. Hammiche and H. M. Pollock, *Int. J. Pharm.*, 1999, **192**, 85–96.
6 B. E. Belkerk, M. A. Soussou, M. Carette, M. A. Djouadi and Y. Scudeller, *J. Phys. D: Appl. Phys.*, 2012, **45**, 295303.
7 D. G. Cahill, H. E. Fischer, T. Klitsner, E. T. Swartz and R. O. Pohl, *J. Vac. Sci. Technol., A*, 1989, **7**, 1259–1266.
8 J. H. Lienhard IV and J. H. Lienhard V, *A Heat Transfer Textbook*, Phlogiston Press, Cambridge, Massachusetts, U.S.A., 4th edn, 2015.
9 A. M. Marconnet, M. Asheghi and K. E. Goodson, *J. Heat Transfer*, 2013, **135**, 061601.
10 C. J. Gomes, M. Madrid, J. V. Goicochea and C. H. Amon, *J. Heat Transfer*, 2006, **128**, 1114–1121.
11 C. Jeong, S. Datta and M. Lundstrom, *J. Appl. Phys.*, 2012, **111**, 1–6.
12 K. E. Goodson and Y. S. Ju, *Annu. Rev. Mater. Sci.*, 1999, **29**, 261–293.
13 D. G. Cahill, K. Goodson and A. Majumdar, *J. Heat Transfer*, 2002, **124**, 223–241.
14 G. Chen, *IEEE Trans. Compon. Packag. Technol.*, 2006, **29**, 238–246.
15 J. S. Reparaz, E. Chavez-Angel, M. R. Wagner, B. Graczykowski, J. Gomis-Bresco, F. Alzina and C. M. S. Torres, *Rev. Sci. Instrum.*, 2014, **85**, 034901.
16 S.-M. Lee and D. G. Cahill, *J. Appl. Phys.*, 1997, **81**, 2590–2595.
17 R. Heiderhoff, H. Li and T. Riedl, *Microelectron. Reliab.*, 2013, **53**, 1413–1417.
18 H. B. G. Casimir, *Physica*, 1938, **6**, 495–500.
19 M. E. Siemens, Q. Li, R. Yang, K. A. Nelson, E. H. Anderson, M. M. Murnane and H. C. Kapteyn, *Nat. Mater.*, 2010, **9**, 26–30.
20 S. Shen, A. Narayanaswamy and G. Chen, *Nano Lett.*, 2009, **9**, 2909–2913.
21 K. Kim, B. Song, V. Fernández-Hurtado, W. Lee, W. Jeong, L. Cui, D. Thompson, J. Feist, M. T. H. Reid, F. J. García-Vidal, J. C. Cuevas, E. Meyhofer and P. Reddy, *Nature*, 2015, **528**, 387–391.
22 A. Majumdar, *J. Heat Transfer*, 1993, **115**, 7–16.
23 P. B. Allen, arXiv:1308.2890, 2013, pp. 1–5.
24 V. Chiloyan, L. Zeng, S. Huberman, A. A. Maznev, K. A. Nelson and G. Chen, *Phys. Rev. B*, 2016, **93**, 155201.
25 J. Meyer, P. Görrn, F. Bertram, S. Hamwi, T. Winkler, H.-H. Johannes, T. Weimann, P. Hinze, T. Riedl and W. Kowalsky, *Adv. Mater.*, 2009, **21**, 1845–1849.
26 R. Heiderhoff, in *2012 19th IEEE International Symposium on the Physical and Failure Analysis of Integrated Circuits*, IEEE, 2012, pp. 1–4.
27 A. Altes, R. Heiderhoff and L. J. Balk, *J. Phys. D: Appl. Phys.*, 2004, **37**, 952–963.
28 A. Altes, R. Tilgner, M. Reissner, G. Steckert and G. Neumann, *Microelectron. Reliab.*, 2008, **48**, 1273–1278.
29 A.-K. Geinzer, *Thermoelastic analysis of devices by scanning near-field thermal microscopy techniques*, University of Wuppertal, 2010.

Open Access Article. Published on 03 October 2016. Downloaded on 6/5/2026 9:49:26 AM.
This article is licensed under a Creative Commons Attribution 3.0 Unported Licence.

30 R. Heiderhoff and L. J. Balk, in *Handbook of Nanoscopy*, ed. G. Van Tendeloo, D. Van Dyck and S. J. Pennycook, Wiley-VCH Verlag & Co. KGaA, Weinheim, Germany, 2012, vol. 1, pp. 499–538.
31 D. G. Cahill, *Rev. Sci. Instrum.*, 1990, **61**, 802–808.
32 G. B. M. Fiege, A. Altes, R. Heiderhoff and L. J. Balk, *J. Phys. D: Appl. Phys.*, 1999, **13**, L13–L17.
33 A. A. Wilson, M. Muñoz Rojo, B. Abad, J. A. Perez, J. Maiz, J. Schomacker, M. Martín-Gonzalez, D.-A. Borca-Tasciuc and T. Borca-Tasciuc, *Nanoscale*, 2015, **7**, 15404–15412.
34 A. Cappella, J.-L. Battaglia, V. Schick, A. Kusiak, A. Lamperti, C. Wiemer and B. Hay, *Adv. Eng. Mater.*, 2013, **15**, 1046–1050.
35 D. G. Cahill and R. O. Pohl, *Phys. Rev. B: Condens. Matter Mater. Phys.*, 1987, **35**, 4067–4073.
36 P. Tovee, M. Pumarol, D. Zeze, K. Kjoller and O. Kolosov, *J. Appl. Phys.*, 2012, **112**, 114317.
37 N. Oka, R. Arisawa, A. Miyamura, Y. Sato, T. Yagi, N. Taketoshi, T. Baba and Y. Shigesato, *Thin Solid Films*, 2010, **518**, 3119–3121.
38 E. T. Swartz and R. O. Pohl, *Rev. Mod. Phys.*, 1989, **61**, 606–668.
39 L. Zhang and A. Chopelas, *Phys. Earth Planet. Inter.*, 1994, **87**, 77–83.
40 F. F. Freeman and A. C. Anderson, *Phys. Rev. B: Condens. Matter Mater. Phys.*, 1986, **34**, 5684–5690.
41 Z. Tian, K. Esfarjani, J. Shiomi, A. S. Henry, G. Chen, Z. Tian, K. Esfarjani, J. Shiomi, A. S. Henry and G. Chen, *Appl. Phys. Lett.*, 2011, **99**, 1–3.
42 D. Xiong, Y. Zhang and H. Zhao, *Phys. Rev. E: Stat., Nonlinear, Soft Matter Phys.*, 2013, **88**, 052128.
43 A. Mittal and S. Mazumder, *J. Heat Transfer*, 2010, **132**, 52402.
44 C. S. Gorham, J. T. Gaskins, G. N. Parsons, M. D. Losego and P. E. Hopkins, *Appl. Phys. Lett.*, 2014, **104**, 253107.
45 M. A. Caravaca, R. A. Casali, J. C. Miño, L. E. Kosteski and R. B. D. Ambra, *e-Proceedings Online Workshop: SimNDT 2010*, 2010.
46 C. B. Carter and M. G. Norton, in *Ceramic Materials*, ed. C. B. Carter and M. G. Norton, Springer New York, New York, NY, 2013, pp. 641–657.